

Cite this: *Soft Matter*, 2012, **8**, 1628

www.rsc.org/softmatter

PAPER

Dynamics of highly concentrated protein solutions around the denaturing transition†

Marcus Hennig,^{‡ab} Felix Roosen-Runge,^b Fajun Zhang,^b Stefan Zorn,^b Maximilian W. A. Skoda,^c Robert M. J. Jacobs,^d Tilo Seydel^{*a} and Frank Schreiber^b

Received 23rd August 2011, Accepted 20th October 2011

DOI: 10.1039/c1sm06609a

Using both quasi-elastic and fixed-window neutron spectroscopy, we study the dynamics of highly concentrated aqueous protein solutions of *bovine serum albumin* around the denaturing transition. For the temperature range 280 K < T < 370 K, the total mean-squared displacement $\langle u^2 \rangle$ is recorded. Below and above the denaturing, we observe that $\langle u^2 \rangle$ increases monotonically with T , but at the denaturing transition it decreases strongly. This observation can be rationalized and quantitatively modeled as a transition from a liquid protein solution to a gel-like state. Atomic vibrations, molecular subunit diffusion and, most importantly, diffusion of the entire protein determine $\langle u^2 \rangle$. The latter is strongly hindered due to entanglement and cross-linking of the chains and causes the pronounced decrease of $\langle u^2 \rangle$. Using information from the full quasi-elastic signal, we separate the diffusion contribution from $\langle u^2 \rangle$ and reveal the transition temperature. For the analysis of this separation, we introduce a general concept, which is applicable to other colloid systems exhibiting both center-of-mass and internal dynamics.

1 Introduction

Crucial to the physical understanding of soft and biological matter is the obvious, but in general insufficiently understood, link between the microscopic properties and the functionality of the system. Microscopic properties, such as dynamics, have been intensely addressed by, *inter alia*, neutron spectroscopy techniques.^{1–4} Neutron spectroscopy allows both the picosecond subunit diffusion and the nanosecond translational and rotational diffusion of globular proteins to be probed.^{5,6} A significant amount of work on protein dynamics has been carried out on powder or hydrated powder samples,² which simplifies the analysis, since some degrees of freedom including the center-of-mass motion do not contribute. Solutions of proteins^{5,7–12} are obviously more complex, but closer to physiological conditions. Importantly, in many situations in biology, proteins are found at rather high concentrations, known as macromolecular crowding, up to and above 30% in volume. This implies that, in contrast to dilute aqueous solutions with effectively independent proteins,

the interactions between the dissolved proteins are important and give rise to qualitatively different effects.

At elevated temperatures proteins denature and at sufficiently high protein concentration aggregate and form gels.^{13,14} The denaturing transition itself is an important key to the physical behavior of the protein.

The issue of denaturing of a protein in a crowded environment was previously addressed by simulation,¹⁵ concluding that crowding can enhance the structural stability, but experimentally the effects arising upon denaturing of crowded proteins with their intrinsic complex charge distribution are not clear. Only few experimental results on the microscopic dynamics of protein suspensions around denaturation are available,^{16,17} but a systematic understanding and a theoretical framework have not been achieved yet. In this study, we report on a neutron spectroscopy study of the denaturing transition of bovine serum albumin (BSA) in crowded aqueous (D₂O) solutions and a newly developed framework to quantitatively investigate the *hindered* dynamics of the proteins upon entanglement and cross-linking and to analyze the different contributions to the mean-squared displacement $\langle u^2 \rangle$ around the denaturing transition. Importantly, our novel framework is not restricted to the study of denaturing of proteins, but can be applied to any system with both center-of-mass and internal dynamics, *e.g.* also conventional polymer solutions.

2 Experimental method and data processing

For all neutron measurements the samples were prepared by dissolving BSA (Sigma-Aldrich product code A3059, 99%

^aInstitut Laue-Langevin, 6 Rue Jules Horowitz B.P. 156, F-38042 Grenoble, France. E-mail: seydel@ill.eu; Tel: +33 476 20 75 79

^bUniversität Tübingen, Institut für Angewandte Physik, Auf der Morgenstelle 10, D-72076 Tübingen, Germany

^cISIS, Rutherford Appleton Laboratory, Chilton, Didcot, OX11 0QX, UK

^dDepartment of Chemistry, Chemistry Research Laboratory, University of Oxford, Mansfield Road, Oxford, OX1 3TA, UK

† Electronic supplementary information (ESI) available. See DOI: 10.1039/c1sm06609a

‡ Current address: Bragg Institute, Australian Nuclear Science and Technology Organization, Locked Bag 2001, Kirrawee DC, NSW 2232, Australia

purity) with mass m in D_2O with volume V to obtain the protein concentration $c = m/V$. After complete dissolution and equilibration, the solutions were contained in double-walled aluminum cylinders with 23 mm outer diameter and 0.3 mm gap which were sealed against vacuum. Due to the complete filling and sealing of these sample holders, the neutron scattering experiments were performed at constant sample volume while the pressure changes with sample temperature. We used the neutron backscattering spectrometers IN10 and IN16 at the ILL in Grenoble in the standard configuration with unpolished Si (111)-monochromator and analyzer crystals, which set the selected neutron wavelength to 6.27 Å and achieve an energy resolution of approximately $\hbar \Delta\omega = 0.9 \mu\text{eV}$ (gaussian FWHM). The Q -ranges set the probed length scales to $3.2 \text{ \AA} \leq l \leq 12 \text{ \AA}$ (IN10) and $3.3 \text{ \AA} \leq l \leq 33 \text{ \AA}$ (IN16), respectively, with $l = 2\pi/Q$. The data were normalized to the incident neutron flux. Using Paalman–Pings coefficients¹⁸ the empty cylinder signal was subtracted. Subsequently, all data were scaled by the inverse detector efficiency obtained from the elastic intensity of vanadium. Due to the large incoherent scattering cross-section of the proteins, our data reflect the single particle correlation function of the protein hydrogen atoms. For the quasi-elastic data, we assume that vibrational and diffusive modes are uncoupled and obtain^{6,10,19,20}

$$S(Q, \omega) = \exp\left(-\frac{1}{3}\langle u_{\text{vib}}^2 \rangle Q^2\right) \mathcal{L}(\omega, \gamma) \otimes \{A(Q) \delta(\omega) + [1 - A(Q)] \mathcal{L}_\beta(\omega, \Gamma)\}. \quad (1)$$

Therein, $\langle u_{\text{vib}}^2 \rangle$ denotes the so-called mean-squared displacement of vibrations. The Lorentzian function $\mathcal{L}(\omega, \gamma)$ models the convolution of translational and rotational diffusion of the entire protein.¹⁰ The symbol \otimes indicates the convolution with respect to the variable ω . $A(Q)$ is the incoherent elastic structure factor. Using a single phenomenological parameter $0 \leq \beta \leq 1$, the Kohlrausch–Williams–Watts (KWW) function²¹

$$\mathcal{L}_\beta(\omega, \Gamma) = \int_{-\infty}^{\infty} \frac{dt}{2\pi} e^{-i\omega t} \exp(-|t \Gamma|^\beta), \quad (2)$$

describes a broad range of internal relaxation times. Although in our case it turns out that $\beta = 1$, we introduce the KWW function to make our analysis applicable to other colloid systems exhibiting both center-of-mass and internal dynamics. Γ and β are assumed to be nearly constant for $Q < 2 \text{ \AA}^{-2}$.^{22,23} Finally, $\delta(\omega)$ designates the Dirac function of the elastic scattering.

The experimental quasi-elastic scattering function reads

$$S_{\text{exp}}(Q, \omega) = \mathcal{R}_{\Delta\omega}(\omega) \otimes S(Q, \omega) + B \quad (3)$$

with the instrumental resolution function $\mathcal{R}_{\Delta\omega}(\omega)$ and a flat background B accounting for both the water diffusion and the phonon contribution which exceed the accessible dynamic range of the instrument.

With fixed elastic window neutron backscattering, one measures the incoherent scattering function at $\omega = 0$ within the instrumental resolution function $\mathcal{R}_{\Delta\omega}(\omega)$. Thus, the measured fixed-window scattering is linked to the quasi-elastic signal by

$$S(Q, |\omega| < \Delta\omega) := \mathcal{R}_{\Delta\omega}(\omega) \otimes S(Q, \omega)|_{\omega=0} = \int \mathcal{R}_{\Delta\omega}(\omega) S(Q, \omega) d\omega. \quad (4)$$

3 Results and discussion

In Fig. 1, the measured fixed-window scattering intensity is shown for a full temperature scan through the denaturing transition for an aqueous BSA solution with $c = 500 \text{ mg ml}^{-1}$ corresponding to a volume fraction of 27%. The change of the overall dynamics is clearly reflected in the non-monotonous behaviour of the intensities *versus* temperature. In order to understand the dynamical changes in more detail, we determine the total mean-square displacement for each temperature, respectively:

$$\langle u^2 \rangle := -3 \lim_{Q \rightarrow 0} \left\{ \frac{\log[S(Q, |\omega| < \Delta\omega)]}{Q^2} \right\}. \quad (5)$$

$\langle u^2 \rangle$ consists of three contributions from atomic vibrations $\langle u_{\text{vib}}^2 \rangle$, molecular subunit diffusion $\langle u_{\text{sub}}^2 \rangle$ and, most importantly, diffusion of the entire protein $\langle u_{\text{diff}}^2 \rangle$ (for a detailed derivation see the Appendix):

$$\langle u^2 \rangle = \langle u_{\text{vib}}^2 \rangle + \langle u_{\text{sub}}^2 \rangle + \langle u_{\text{diff}}^2 \rangle \quad (6)$$

$$\langle u_{\text{sub}}^2 \rangle = (1 - p)\chi \langle \Delta r^2 \rangle \quad (7)$$

$$\langle u_{\text{diff}}^2 \rangle = (2\pi)^{-3/2} 6D\tau, \quad (8)$$

with $\chi = 1 - \sqrt{2/\pi} \int_0^\infty \exp(-\xi^2/2 - |y \xi|^\beta) d\xi$, where $y = \frac{\Gamma}{\Delta\omega}$.

For our data $\chi \approx 1$, since for high-resolution instruments we can safely assume that $\Gamma \gg \Delta\omega$. A fraction p of protons has a correlation time far beyond the accessible time window, such that they have a very narrow energy signal and, therefore, can be considered as immobile. The internal diffusive modes are confined on the given time scale to an average length of $\langle \Delta r^2 \rangle^{1/2}$. The mean-squared displacement due to diffusion of the entire protein is $6D\tau$, where $\tau = 2\pi/\Delta\omega$ is the maximum observation

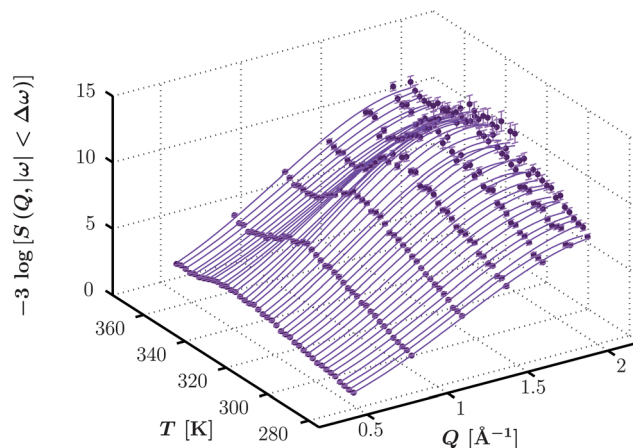


Fig. 1 Elastic intensity $S(Q, |\omega| < \Delta\omega)$ (solid circles) of a 500 mg ml⁻¹ BSA aqueous (D_2O) solution upon heating from 280 to 370 K with $7.4 \times 10^{-2} \text{ K min}^{-1}$. The data were recorded at IN10. Fits of the polynomial eqn (10) to the data at fixed temperatures are superimposed as solid lines.

time of the instrument and D is the apparent diffusion coefficient taking into account both rotational and translational diffusion.¹¹

Fig. 2 (A) shows $\langle u^2 \rangle$ for the full temperature scan through the denaturation transition. $\langle u^2 \rangle$ was extracted from the data by a quadratic fit to $\log[S(Q,|\omega| < \Delta\omega)]$ versus Q^2 (eqn (10)) using the entire Q -range of IN10, as shown for one example data set in the inset. Starting at $T = 280$ K, $\langle u^2 \rangle$ increases linearly with temperature up to 325 K. A steep decrease is observed in the temperature range of denaturing, namely 331 K $< T < 354$ K, consistent with structural changes observed by Fourier transform infrared spectroscopy.²⁴ Upon further heating, $\langle u^2 \rangle$ starts to increase again with temperature. $\langle u^2 \rangle$ is significantly larger than the typical observed vibrational amplitude of only 10^{-2} Å², suggesting that protein diffusive modes are present in addition to atomic vibrations confirming the validity of eqn (6). We rationalize the data depicted in Fig. 2 (A), remembering that below the denaturation temperature, proteins occur in their native state, which for most globular proteins is a solution of charge-stabilized monomers.^{25,26} The protein dynamics in this region consists of global translational and rotational diffusion, internal and confined diffusive motion of side chains and protein domains

and vibrational modes. Upon increasing the temperature, the proteins enter the denaturation regime ($T_1 < T < T_2$). We rationalize this transition in two steps. First, the proteins unfold and extend, which can be understood as similarly to a helix to random coil transition, initially proposed in the seminal paper by Zimm and Bragg.²⁷ Second, the unfolded protein chains entangle and potentially cross-link partly. This entanglement and cross-linking process can be seen as in between chemical gelation and polymer vulcanization.^{28,29} The entanglement significantly reduces translational and rotational diffusion. While a quantitative theory of the amplitude (Δu^2 in the model described below) of the effect is not available at present, we can qualitatively use the analogy to existing theories for the cross-linking of polymers (vulcanization).³⁰ The segment dynamics is then reduced typically by (some power of) the inverse number of entanglement points, N_e , and it appears plausible that a similar mechanism is at work also for concentrated protein solutions. Thus, raising the temperature above the denaturation regime, a gel-like state is observed which can be understood rather in terms of the dynamics of a cross-linked network than in terms of the dynamics of separated molecules. In the spirit of the above, we model the dynamics of the transition by

$$\langle u^2 \rangle = (a_1 T + b_1)[1 - \Theta(T^*)] + (a_2 T + b_2)\Theta(T^*) \quad (9)$$

where $T^* = (T - T_0)/\Delta T$ with the transition width ΔT and the denaturing temperature T_0 . The indices 1 and 2 denote the liquid state of native proteins and gel-like state of denatured proteins, respectively, and $\Theta(x)$ is a smeared-out step function, $\Theta(x) = [1 + \exp(-x)]^{-1}$, with the functional characteristics of the helix melting models by Zimm and Bragg.²⁷ For the case $a_1 = a_2$, which is approximately fulfilled here, the temperatures $T_{1,2}$ of the turning points of $\langle u^2 \rangle$, defining the denaturing interval, are $T_{1,2} = T_0 \pm \Delta T \ln[z + \sqrt{z(z-2)} - 1]$, where $\Delta u^2 = b_1 - b_2$ and $z = \frac{\Delta u^2}{2 a \Delta T}$. T_1 can be interpreted as the temperature where unfolding of the proteins starts, and T_2 where the entanglement and cross-linking of the chains is completed. $\Delta u^2/\Delta T$ is a measure of how rapidly $\langle u^2 \rangle$ decreases. The width ΔT of the transition in a simple model depends on the inverse number of participating units of the helix, but of course for a real protein this is more complex. The reduction Δu^2 of the dynamics is due to entanglement. Although we observe that the slopes a_i are nearly the same below and above denaturing, we point out that in the general case, a_i probably depends on the protein concentration. Note, when the gel-like state is cooled back from 370 K down to 280 K, the curve for $T < T_2$ of $\langle u^2 \rangle$ is well below the heating curve in Fig. 2 (A),³¹ which shows the irreversibility of the denaturing process and supports the assumption that translational and rotational diffusion are significantly hindered by entanglement and cross-links. Hence, upon cooling the cross-linked network of denatured proteins persists.

In order to unveil the temperature dependence of $\langle u^2 \rangle - \langle u_{\text{diff}}^2 \rangle$, namely the cumulative mean-squared displacement originating only from vibrational and subunit-diffusive modes, we use the apparent diffusion coefficient D extracted from quasi-elastic spectra to calculate the corresponding contribution to $\langle u^2 \rangle$ by eqn (8). Fig. 3 shows a typical spectrum recorded on IN16.

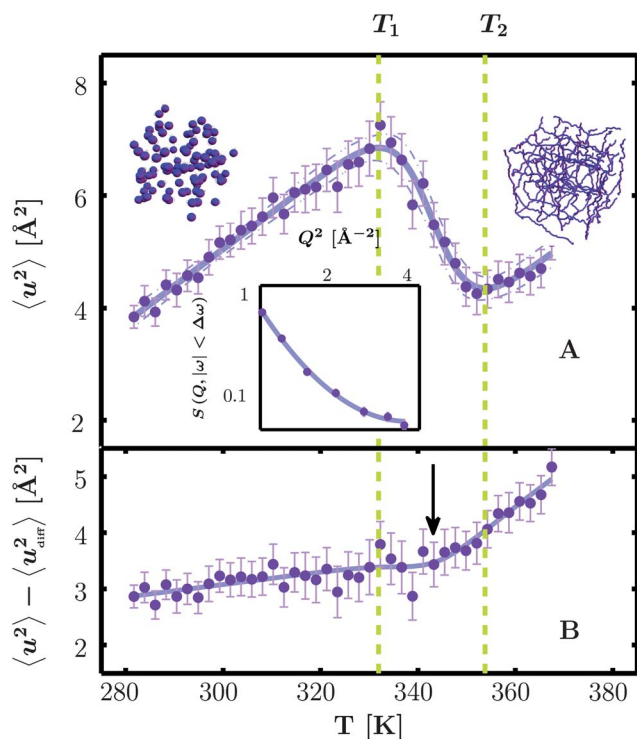


Fig. 2 (A) Total mean-squared displacement $\langle u^2 \rangle$ (circles) of an aqueous BSA (500 mg ml⁻¹) solution versus temperature T . The solution was heated at 7.4×10^{-2} K min⁻¹. Using eqn (9) we describe the data (solid line superimposed on the data) and determine the denaturing interval $T_1 < T < T_2$ (dotted vertical lines). The upper images illustrate a colloidal suspension of native proteins (left) and the cross-linked network of denatured proteins (right). Inset: Measured elastic intensity $S(Q,|\omega| < \Delta\omega)$ versus Q^2 (circles) for the same sample at $T = 290$ K recorded at IN10. A quadratic fit according to eqn (10) (solid line) was used to determine $\langle u^2 \rangle$. (B) $\langle u^2 \rangle - \langle u_{\text{diff}}^2 \rangle$ (circles). The two vertical dashed lines denote the transition regime. At $T_0 = (T_1 + T_2)/2$ a transition occurs, characterized by a kink in the curve (arrow).

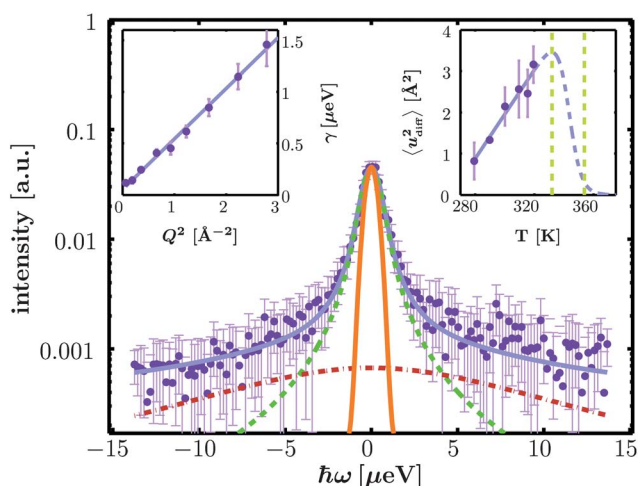


Fig. 3 Example spectrum $S(Q, \omega)$ (symbols) recorded at IN16 for BSA in D_2O (protein concentration 500 mg ml^{-1} corresponding to a volume fraction $\phi = 27\%$, $T = 301 \text{ K}$, individual detector tube at $Q = 0.6 \text{ \AA}^{-1}$). The solid line superimposed on the data indicates the fit of the model from eqn (3) with $\beta = 1$, hence the KKW function turns into to Lorentzian $\mathcal{L}(\omega, \Gamma)$. The Lorentzians in eqn (3) are indicated by the dashed $[\mathcal{R}(\omega) \otimes \mathcal{L}(\omega, \gamma)]$ and dash-dotted $[\mathcal{R}(\omega) \otimes \mathcal{L}(\omega, \gamma + \Gamma)]$ lines, respectively. The solid line in the center denotes a Gaussian model of the resolution function $\mathcal{R}(\omega)$. The scattering signal decreases with Q , resulting in larger error bars on the fitted γ . Inset left: γ (symbols) fitted to the signal from grouped detectors versus Q^2 . Inset right: Temperature dependence of $\langle u_{\text{diff}}^2 \rangle$ due to global diffusion as calculated from eqn (8) (symbols). The solid line is a linear fit for $T \leq 320 \text{ K}$, namely $\langle u_{\text{diff}}^2 \rangle = aT + b$. For temperatures beyond 320 K we assume that the diffusion is hindered by entanglement of the proteins and, hence, nearly zero. Therefore, we postulate $\langle u_{\text{diff}}^2 \rangle = (aT + b)[1 - \Theta(T^*)]$. The transition regime is denoted by the two vertical dashed lines.

The width γ as obtained from the fits to eqn (3) are plotted in the left-hand inset of Fig. 3. We observe a clear relationship $\gamma = DQ^2$ defining the apparent diffusion coefficient D . Considering that not only the translational but also the rotational diffusion contributes to D ,^{10,11} we can interpret D as a measure for the global diffusive dynamics of the protein. The right-hand inset in Fig. 3 depicts the temperature dependence of the mean-squared displacement $\langle u_{\text{diff}}^2 \rangle$ calculated from eqn (8) using the energy resolution $\hbar\Delta\omega = 0.9 \text{ \mu eV}$. Below the transition regime, indicated by the two vertical lines, we observe a linear relation $\langle u_{\text{diff}}^2 \rangle = aT + b$. Inspired by de Gennes' scaling law for the diffusion of a polymer in a cross-linked network,³⁰ we assume a negligible global diffusion coefficient D for $T > T_2$. Indeed, near and above the denaturing temperature, fitting according to eqn (3) yields diffusion coefficients D dropping close to zero. Therefore, we describe the full temperature dependence by $\langle u_{\text{diff}}^2 \rangle = (aT + b)[1 - \Theta(T^*)]$, where $\Theta(T^*)$ is the same smeared-out step function used for the fit of $\langle u^2 \rangle$ as shown in Fig. 2 (A). Fig. 2 (B) depicts the temperature dependence of the mean-squared displacement $\langle u^2 \rangle - \langle u_{\text{diff}}^2 \rangle$. We observe a change of the dynamics at a temperature $T_0 = 343 \text{ K}$ characterizing the transition from a liquid protein solution to a gel-like state. The inverse slopes of $\langle u^2 \rangle - \langle u_{\text{diff}}^2 \rangle$ versus T , occasionally discussed in the literature as a phenomenological force constant,³² are $k_1 = (a_1 - a)^{-1} = 4.1 \times 10^{-2} \text{ N m}^{-1}$ and $k_2 = a_2^{-1} = 0.7 \times 10^{-2} \text{ N m}^{-1}$, for $T < T_1$

and $T > T_2$, respectively. We note that the physical significance of the force constant is limited in the present case, but it is stated for reasons of comparability.

We speculate that the difference in k_1 and k_2 can be attributed to the higher conformational flexibility of the unfolded protein chains in the cross-linked network. In the native state the proteins are stiffer due to hydrogen bonds and surface charge both of which are mainly responsible for the stable three-dimensional structure.

4 Summary and conclusion

We investigated the dynamics of crowded BSA protein solutions around the denaturing transition. We have identified denaturing in the fixed-window data. We have developed a novel physical framework for the unfolding and entanglement allowing $\langle u^2 \rangle(T)$ to be understood. Using quasi-elastic and fixed-window scattering data, the measured $\langle u^2 \rangle$ can be decomposed into the vibrational, subunit diffusive, and global diffusive contributions. The characteristic transition temperatures defining the denaturation range become observable. The driving force for the drop in $\langle u^2 \rangle$ in the denaturing regime can be rationalized by the significant slowdown of the global diffusion, accounting for both translational and rotational diffusion. This slowdown is induced by structural change and entanglement as well as cross-linking of the proteins. The experimental and analytical framework, which we have introduced, will allow to accurately test computer models.¹⁵

Appendix: Analysis of fixed elastic window neutron backscattering

In this appendix we develop an analytic framework for the calculation and decomposition of the total mean squared displacement $\langle u^2 \rangle$ of a protein in solution determined with fixed elastic window neutron backscattering. The presented analysis is based on quasi-elastic concepts, which are transferred to the case of fixed elastic window measurements.

Assuming the independence of diffusive and vibrational modes, as well as the harmonicity of the latter, eqn (1) expresses the full quasi-elastic scattering function of a protein solution, $S(Q, \omega)$, accounting for translational and rotational diffusion.¹⁰ The so-called elastic intensity of proteins in solution, $S(Q, |\omega| < \Delta\omega)$, is directly related *via* the resolution function, as given in eqn (4).

Anticipating the result from the derivation subsequent to this section, the total mean-squared displacement $\langle u^2 \rangle$ is obtained from the elastic intensity by fitting $-3\log[S(Q, |\omega| < \Delta\omega)]$ with the following polynomial:

$$P(Q) = b + \langle u^2 \rangle Q^2 + cQ^4 \quad (10)$$

Therein, b accounts for both the background and the arbitrary scaling of the experimental elastic line, c originates from higher spatial correlations as described in detail in the next section.

Connection of elastic scattering intensity to several diffusive modes

In the following, we derive a formula describing the elastic line intensity in terms of vibrational, global and internal diffusive

modes for small Q values. To start with, we solve the integral eqn (4) by using the model function eqn (1) and assume a Gaussian resolution function of the instrument (which is valid for the spectrometers IN10 and IN16) of the form

$$\mathcal{R}_{\Delta\omega}(\omega) = \exp\left(-\frac{\omega^2}{2\Delta\omega^2}\right).$$

Thereby, for reasons of readability we skip any scaling parameter. With this the integral eqn (4) yields

$$S(Q, |\omega| < \Delta\omega) = \exp\left(-\frac{1}{3}\langle u_{\text{vib}}^2 \rangle Q^2\right) \cdot \left\{ A(Q) F_1\left(\frac{\gamma}{\Delta\omega}, 0\right) + [1 - A(Q)] F_\beta\left(\frac{\gamma}{\Delta\omega}, \frac{\Gamma}{\Delta\omega}\right) \right\}, \quad (11)$$

where F_β is the integral expression

$$F_\beta(x, y) = \sqrt{\frac{2}{\pi}} \exp\left(\frac{x^2}{2}\right) \int_0^\infty \exp\left[-\frac{1}{2}(\xi + x)^2 - |y \xi|^\beta\right] d\xi.$$

General mean-squared displacement

The total mean-squared displacement $\langle u^2 \rangle$ is introduced as an apparent quantity in eqn (5). In the following we will attach a physical meaning to it. In order to analyze $\langle u^2 \rangle$, we define the general (Q -dependent) mean-squared displacement $\langle u^2 \rangle_Q$ by

$$\exp\left[-\frac{Q^2}{3}\langle u^2 \rangle_Q\right] := S(Q, |\omega| < \Delta\omega). \quad (12)$$

Note that the explicit Q -dependence is denoted by a subscript Q to distinguish it from the total mean-squared displacement $\langle u^2 \rangle$. Using eqn (12) and eqn (11), we obtain

$$\langle u^2 \rangle_Q = \langle u_{\text{vib}}^2 \rangle - \frac{3}{Q^2} \log \xi(Q), \quad (13)$$

in which

$$\xi(Q) = A(Q) F_1\left(\frac{\gamma}{\Delta\omega}, 0\right) + [1 - A(Q)] F_\beta\left(\frac{\gamma}{\Delta\omega}, \frac{\Gamma}{\Delta\omega}\right).$$

We approximate eqn (13) up to 3rd order using a Taylor polynomial at $Q = 0$:

$$\langle u^2 \rangle_Q = \sum_{n=0}^3 \frac{a_n}{n!} Q^n + \mathcal{O}(Q^4). \quad (14)$$

Therein, $\mathcal{O}(Q^4)$ is the remainder of the series and the coefficients are defined by

$$a_n = \lim_{Q \rightarrow 0} \frac{d^n}{dQ^n} \langle u^2 \rangle_Q.$$

n^{th} -Derivative of incoherent elastic structure factor

In order to calculate the Taylor coefficients a_n , we have to first determine the n^{th} -derivative of the incoherent elastic structure factor. To start with, we introduce a general form of the incoherent elastic structure factor, which according to Bée³³ reads

$$B(\mathbf{Q}) = \frac{1}{N} \sum_{j=1}^N \left| \langle e^{i\mathbf{Q}\mathbf{r}_j} \rangle \right|^2.$$

Therein, $\mathbf{r}_j = (x_j, y_j, z_j)^T$ might be the position vector of the j^{th} scatterer in one of the solvent exposed side chains of the protein. We recall that a protein in solution has no preferential orientation vector due the random collisions with the surrounding solvent molecules. We assume that the orientations of the molecules are nearly equally distributed. Therefore, we have to average the general elastic incoherent structure factor $A(Q)$ over all possible orientations yielding

$$A_0(Q) = \frac{1}{4\pi} \int_0^{2\pi} \int_0^\pi B(\mathbf{Q}) \sin\theta \, d\theta \, d\varphi.$$

in which $\mathbf{Q} = Q[\cos(\varphi)\sin(\theta), \sin(\varphi)\sin(\theta), \cos(\theta)]^T$. For reasons of generality we additionally consider the pseudo-elastic incoherent structure factor,^{16,22} based on the following conception: Correlation times much longer than the instrumental time window correspond to a very narrow signal in ω , which is indistinguishable from the elastic peak in the quasi-elastic signal. Therefore, a fraction p of scatterers is considered as immobile, the remaining fraction $1 - p$ as diffusive scatterers. This translates into the pseudo-elastic incoherent structure factor

$$A(Q) = p + (1 - p) A_0(Q)$$

The first five derivatives of $A(Q)$, denoted by $A^{(n)}(Q)$, were obtained by employing *Mathematica*[®] for the limit $Q = 0$:

$$\begin{aligned} A(0) &= 1 \\ A^{(1)}(0) &= 0 \\ A^{(2)}(0) &= -\frac{2(1-p)}{3} \langle \Delta\mathbf{r}^2 \rangle \\ A^{(3)}(0) &= 0 \\ A^{(4)}(0) &= \frac{1-p}{5} (m_x + m_y + m_z + 2m_{x,y} + 2m_{x,z} + 2m_{y,z}) \\ A^{(5)}(0) &= 0, \end{aligned} \quad (15)$$

where

$$\langle \Delta\mathbf{r}^2 \rangle = \frac{1}{N} \sum_{j=1}^N \langle (\mathbf{r}_j - \langle \mathbf{r}_j \rangle)^2 \rangle$$

is the average fluctuation amplitude, related to the size of the confinement of the internal diffusive scatterer, such as the protein side chains. Moreover, the higher moments of the scattering coordinates are

$$\begin{aligned} m_x &= \frac{2}{N} \sum_{j=1}^N \left(\langle x_j^4 \rangle + 3 \langle x_j^2 \rangle^2 - 4 \langle x_j^3 \rangle \langle x_j \rangle \right) \\ m_{x,y} &= \frac{2}{N} \sum_{j=1}^N \left(2 \langle x_j y_j \rangle^2 - 2 \langle y_j \rangle \langle x_j^2 y_j \rangle \right. \\ &\quad \left. + \langle x_j^2 \rangle \langle y_j^2 \rangle - 2 \langle x_j \rangle \langle x_j y_j^2 \rangle + \langle x_j^2 y_j^2 \rangle \right). \end{aligned}$$

We note that the expressions m_y , m_z and $m_{x,z}$, $m_{y,z}$ are analogously defined.

Taylor coefficients a_n

Having obtained the n^{th} -derivative of the incoherent elastic structure factor $A^{(n)}(0)$, we proceed by calculating the Taylor coefficients in the truncated series (eqn (14)). To this end, we first calculate the derivatives for ξ at $Q = 0$, which are

$$\begin{aligned}\xi(0) &= 1 \\ \xi^{(1)}(0) &= 0 \\ \xi^{(2)}(0) &= -\frac{2D}{\Delta\omega} \sqrt{\frac{2}{\pi}} + \left[1 - F_\beta\left(0, \frac{\Gamma}{\Delta\omega}\right)\right] A^{(2)}(0) \\ \xi^{(3)}(0) &= 0 \\ \xi^{(4)}(0) &= \left[1 - F_\beta\left(0, \frac{\Gamma}{\Delta\omega}\right)\right] A^{(4)}(0) \\ &\quad + \frac{12D^2}{\Delta\omega^2} \left[1 - \frac{\Delta\omega}{D} A^{(2)}(0) \left\{\sqrt{\frac{2}{\pi}} + F_\beta^{(1,0)}\left(0, \frac{\Gamma}{\Delta\omega}\right)\right\}\right] \\ \xi^{(5)}(0) &= 0,\end{aligned}\quad (16)$$

where $F_\beta^{(1,0)}$ denotes the derivative of F_β (eqn (12)) with respect to the first argument. Using $\xi^{(n)}(0)$ we obtain the Taylor coefficients:

$$\begin{aligned}a_0 &= -\frac{3}{2} \xi^{(2)}(0) \\ a_1 &= 0 \\ a_2 &= \frac{1}{4} \left[3 \xi^{(2)}(0)^2 - \xi^{(4)}(0)\right] \\ a_3 &= 0\end{aligned}\quad (17)$$

Finally, the general total mean-squared displacement $\langle u^2 \rangle_Q$ can be approximated as follows

$$\langle u^2 \rangle_Q = a_0 + \frac{a_2}{2} Q^2 + \mathcal{O}(Q^4).\quad (18)$$

Decomposition of total mean-squared displacement

Using eqn (18) the total mean-squared displacement simplifies to (cf. eqn (5))

$$\langle u^2 \rangle := -3 \lim_{Q \rightarrow 0} \left\{ \frac{\log[S(Q, |\omega| < \Delta\omega)]}{Q^2} \right\} = a_0.\quad (19)$$

by combining eqn (17), (16), (15) the total mean-squared displacement can be decomposed into the following sum (cf. eqn (6), (7, 8))

$$\begin{aligned}\langle u^2 \rangle &= \langle u_{\text{vib}}^2 \rangle + \langle u_{\text{sub}}^2 \rangle + \langle u_{\text{diff}}^2 \rangle \\ \langle u_{\text{sub}}^2 \rangle &= (1-p) \chi \langle \Delta \mathbf{r}^2 \rangle \\ \langle u_{\text{diff}}^2 \rangle &= 3 \sqrt{\frac{2}{\pi}} \frac{D}{\Delta\omega^2},\end{aligned}\quad (20)$$

Therein, $\chi = \left[1 - F_\beta\left(0, \frac{\Gamma}{\Delta\omega}\right)\right]$. Due to the energy resolution of the instrument the global diffusion of the protein can only be observed within a time window of width $\tau = 2\pi/\Delta\omega$. During that

time the protein has isotropically explored a space, which size is characterized by a mean-squared displacement of $\langle \Delta \mathbf{R}^2(\tau) \rangle = 6D\tau$. Hence, $\langle u_{\text{diff}}^2 \rangle = (2\pi)^{-3/2} \langle \Delta \mathbf{R}^2(\tau) \rangle$.

Acknowledgements

The authors gratefully acknowledge the allocation of beamtime at the ILL. The authors benefitted from discussions with G. Zaccai and H. Schober.

References

- 1 J. Fitter, T. Gutberlet and J. Katsaras, *Neutron scattering in biology: techniques and applications*, Springer, Berlin Heidelberg, 2006.
- 2 F. Gabel, D. Bicout, U. Lehnert, M. Tehei, M. Weik and G. Zaccai, *Q. Rev. Biophys.*, 2003, **35**, 327–367.
- 3 W. Doster, S. Cusack and W. Petry, *Nature*, 1989, **337**, 754–756.
- 4 S. Longeville, W. Doster and G. Kali, *Chem. Phys.*, 2003, **292**, 413–424.
- 5 M. Bée, *Chem. Phys.*, 2003, **292**, 121–141.
- 6 M. Bée, *Quasielastic neutron scattering*, Adam Hilger, Bristol, 1988.
- 7 C. Caronna, F. Natali and A. Cupane, *Biophys. Chem.*, 2005, **116**, 219–225.
- 8 P. Fenimore, H. Frauenfelder, B. McMahon and R. Young, *Proc. Natl. Acad. Sci. U. S. A.*, 2004, **101**, 14408–14413.
- 9 A. Stadler, I. Digel, G. Artmann, J. Embs, G. Zaccai and G. Büldt, *Biophys. J.*, 2008, **95**, 5449–5461.
- 10 J. Perez, J. Zanotti and D. Durand, *Biophys. J.*, 1999, **77**, 454–469.
- 11 F. Roosen-Runge, M. Hennig, F. Zhang, R. M. J. Jacobs, M. Sztucki, H. Schober, T. Seydel and F. Schreiber, *Proc. Natl. Acad. Sci. U. S. A.*, 2011, **108**, 11815–11820.
- 12 F. Roosen-Runge, M. Hennig, Tilo Seydel, *et al.*, *Biochim. Biophys. Acta, Proteins Proteomics*, 2010, **1804**, 68–75.
- 13 A. Tobitani and S. Ross-Murphy, *Macromolecules*, 1997, **30**, 4845–4854.
- 14 V. Vetri, F. Librizzi, M. Leone and V. Militello, *Eur. Biophys. J.*, 2007, **36**, 717–725.
- 15 A. Kudlay, M. Cheung and D. Thirumalai, *Phys. Rev. Lett.*, 2009, **102**, 118101.
- 16 D. Russo, J. Perez, J. Zanotti and M. Desmadril, *Biophys. J.*, 2002, **83**, 2792–2800.
- 17 G. Gibrat, F. Assairi, Y. Blouquit, C. Craescu and M. C. Bellissent-Funel, *Biophys. J.*, 2008, **95**, 5247–5256.
- 18 H. Paalman and C. Pings, *J. Appl. Phys.*, 1962, **33**, 2635–2639.
- 19 W. Doster, S. Busch, A. M. Gaspar and H. Scheer, *Phys. Rev. Lett.*, 2010, **104**, 098101.
- 20 S. Dellerue, A. J. Petrescu, J. C. Smith and M. C. Bellissent-Funel, *Biophys. J.*, 2001, **81**, 1666–1676.
- 21 G. Williams and D. C. Watts, *Trans. Faraday Soc.*, 1970, **66**, 80–85.
- 22 M. Kataoka, M. Ferrand, A. V. Goupil-Lamy, H. Kamikubo, J. Yunoki, T. Oka and J. C. Smith, *Physica B*, 1999, **266**, 20–26.
- 23 F. Volino and A. Dianoux, *Mol. Phys.*, 1980, **41**, 271–279.
- 24 I. van Stokkum, H. Linsdell and J. Hadden, *Biochemistry*, 1995, **34**, 10508–10518.
- 25 A. Hunter and G. Carta, *J. Chromatogr., A*, 2001, **937**, 13–19.
- 26 F. Zhang, M. W. A. Skoda, R. M. J. Jacobs, R. A. Martin, C. M. Martin and F. Schreiber, *J. Phys. Chem. B*, 2007, **111**, 251–259.
- 27 B. Zimm and J. Bragg, *J. Chem. Phys.*, 1959, **31**, 526–535.
- 28 C. L. Bon, T. Nicolai and D. Durand, *Macromolecules*, 1999, **32**, 6120–6127.
- 29 P. L. San Biagio, D. Bulone, A. Emanuele and M. U. Palma, *Biophys. J.*, 1996, **70**, 494–499.
- 30 P. G. de Gennes, *Scaling concepts in polymer physics*, Cornell University, 1979.
- 31 *Supplementary online material available*.
- 32 G. Zaccai, *Science*, 2000, **288**, 1604–1607.
- 33 M. Bée, *Phys. B*, 1992, **182**, 323–336.